Climate impact on interannual variability of Weddell Sea Bottom Water

Darren C. McKee,[1,2] Xiaojun Yuan,[1] Arnold L. Gordon,[1,2] Bruce A. Huber,[1] and Zhaoqian Dong[3]

Received 24 June 2010; revised 18 February 2011; accepted 3 March 2011; published 26 May 2011.

[1] Bottom water formed in the Weddell Sea plays a significant role in ventilating the global abyssal ocean, forming a central component of the global overturning circulation. To place Weddell Sea Bottom Water in the context of larger scale climate fluctuations, we analyze the temporal variability of an 8-year (April 1999 through January 2007) time series of bottom water temperature relative to the El Niño/Southern Oscillation (ENSO), Southern Annular Mode (SAM), and Antarctic Dipole (ADP). In addition to a pronounced seasonal cycle, the temperature record reveals clear interannual variability with anomalously cold pulses in 1999 and 2002 and no cold event in 2000. Correlations of the time series with ENSO, SAM, and ADP indices peak with the indices leading by 14–20 months. Secondary weaker correlations with the SAM index exist at 1–6 month lead time. A multivariate EOF analysis of surface variables shows that the leading mode represents characteristic traits of out-of-phase SAM and ENSO impact patterns and is well separated from other modes in terms of variance explained. The leading principal component correlates with the bottom water temperature at similar time scales as did the climate indices, implying impact from large-scale climate. Two physical mechanisms could link the climate forcing to the bottom water variability. First, anomalous winds may alter production of dense shelf water by modulating open-water area over the shelf. Second, surface winds may alter the volume of dense water exported from the shelf by governing the Weddell Gyre's cyclonic vigor.

Citation: McKee, D. C., X. Yuan, A. L. Gordon, B. A. Huber, and Z. Dong (2011), Climate impact on interannual variability of Weddell Sea Bottom Water, *J. Geophys. Res.*, *116*, C05020, doi:10.1029/2010JC006484.

1. Introduction

[2] Bottom waters formed in the marginal seas of Antarctica play a significant role in ventilating the global abyssal ocean. The Weddell Gyre facilitates input of source waters to the Weddell Sea, encourages complex modifications through air-sea-ice and ice shelf-water interactions, and serves as a conduit for export via complicated bottom topography. Its global relevance has made the Weddell Gyre the subject of much attention in the past, including studies of trends and interannual variability in either the gyre itself or the surrounding ocean-ice-atmosphere system [e.g., *Fahrbach et al.*, 2004; *Martinson and Iannuzzi*, 2003; *Meredith et al.*, 2008; *Kerr et al.*, 2009; *Lefebvre et al.*, 2004].

[3] The Weddell gyre's cyclonic circulation is partly driven by climatological wind systems over the gyre [*Schroder and Fahrbach*, 1999]. Warm saline waters escape the Antarctic Circumpolar Current near 20°E, where they are carried in the cyclonic gyre to the continental shelf in the southwest, losing heat along the way. There, entrainment with dense shelf water results in the formation of bottom water masses, steered within the cyclonic circulation by topography to their destinations. The densest water mass, Weddell Sea Bottom Water (WSBW), is defined as bottom water with potential temperature (θ°C) less than −0.7°C [*Orsi et al.*, 1993].

[4] Different varieties of WSBW exist with different source properties or formation mechanisms [see *Gordon*, 1998; *Gordon et al.*, 2001; *Huhn et al.*, 2008]. Accepted formation processes can be summarized in two mechanisms. The common requirement is upwelling of saline warm deep water (WDW), cooled sufficiently in winter with increased density from brine rejection. The first process calls for WDW interacting with high-salinity shelf water (HSSW) and winter water (WW) near the shelf break, mixing with further entrainment upon descent [*Foster and Carmack*, 1976]. *Foster and Carmack*'s [1976] mixing scheme suggests WSBW is about 25% shelf water and 62.5% WDW, with the remainder being WW. Isotope data agree rather well with these ratios (about 25% and 70%, respectively)

[1]Lamont-Doherty Earth Observatory, Columbia University, Palisades, New York, USA.
[2]Department of Earth and Environmental Sciences, Columbia University, New York, New York, USA.
[3]Polar Research Institute of China, Shanghai, China.

0148-0227/11/2010JC006484

[*Weppernig et al.*, 1996]. The second process involves HSSW under the southern ice shelves reaching a supercooled (and relatively fresher) state to form ice shelf water (ISW), ultimately capable of descending the slope and mixing with surrounding WDW [*Foldvik et al.*, 1985]. Of these two processes, western shelf water contributes about 2–3 times more to the water column below 0°C than does ISW [*Weppernig et al.*, 1996]. In total, the transport of source waters is about 0.97–2.5 Sv, while the transport of WSBW is about 2–5 Sv [*Carmack and Foster*, 1975; *Foster and Carmack*, 1976; *Fahrbach et al.*, 1995; *Gordon et al.*, 2001; *Grumbine*, 1991].

[5] Various studies have observed a plume-like nature in water mass properties [*Drinkwater et al.*, 1995; *Barber and Crane*, 1995; *von Gyldenfeldt et al.*, 2002; *Foster and Middleton*, 1980], highlighting the roles of cabbeling and thermobaric effects in allowing dense shelf waters to descend the slope [*Gordon et al.*, 1993] as well as the role of seasonality in surface conditions such as sea ice formation and brine rejection [*Drinkwater et al.*, 1995]. Location of the shelf slope front and degree of baroclinicity in the Weddell Gyre [*Meredith et al.*, 2008; *Jullion et al.*, 2010] place further constraints on the export of dense water.

[6] The importance of brine rejection and cyclonic vigor highlight the potential roles of sea ice production over the southwestern continental shelf and cyclonicity of the wind field over the Weddell Sea, respectively, in describing interannual variability of WSBW. The surface forcing from the atmosphere directly affects these two processes. The atmospheric variability at the surface, in turn, is largely controlled by large-scale regional and extrapolar climate variabilities. Particularly, El Niño-Southern Oscillation (ENSO) and the Southern Annular Mode (SAM) have well-documented responses in the ocean-ice-atmosphere system of the Weddell Sea region [*Yuan and Martinson*, 2000, 2001; *Yuan*, 2004; *Martinson and Iannuzzi*, 2003; *Lefebvre and Goosse*, 2005; *Lefebvre et al.*, 2004; *Holland et al.*, 2005]. Such responses could link large-scale climate to the observed variability in WSBW.

[7] For ENSO, while a detailed analysis is shown by *Yuan* [2004], the important result for this study is the presence of a low-pressure anomaly over the Bellingshausen Sea region during cold events with a corresponding high-pressure anomaly during warm events. This yields greater meridional heat flux on the Atlantic side of the peninsula and lesser on the Pacific side in cold events, causing opposite phases of anomalies in ice edge extent, meridional winds, and surface temperature in these two basins, termed as the Antarctic Dipole [*Yuan and Martinson*, 2000; *Yuan*, 2004]. ENSO has an equally significant impact on the vigor of the Weddell Gyre. With warm ENSO events, the gyre center contracts and shifts southward under enhanced cyclonic forcing [*Martinson and Iannuzzi*, 2003].

[8] The Antarctic Dipole (ADP), triggered by ENSO events [*Rind et al.*, 2001; *Yuan*, 2004] and representing the greatest temperature response to ENSO outside the equatorial Pacific [*Liu et al.*, 2002], is the predominant interannual signal in the Southern Ocean sea ice fields [*Yuan and Martinson*, 2001]. Its surface signature is an out-of-phase pattern in the sea ice edge and surface air temperature between the Atlantic and Pacific sectors. Because of the positive feedback within the ocean-ice-atmosphere system in polar seas, the ADP anomalies are amplified and matured after the tropical forcing demises, making it a unique high-latitude mode [*Yuan*, 2004] that sets surface conditions in the Weddell Sea.

[9] The SAM consists of an out-of-phase oscillation in pressure anomalies between middle and high latitudes and is a dominant climate mode in the Southern Hemisphere pressure field [*Gong and Wang*, 1999; *Thompson and Wallace*, 2000]. A positive SAM strengthens westerlies to isolate the Antarctic continent and results in cooling over the continent [*Thompson and Solomon*, 2002] except in the peninsula region where a pressure anomaly causes warming through advection of warmer air in the form of southward winds to the east of the peninsula and northward winds to the west: it is not a perfectly annular mode [*Lefebvre et al.*, 2004]. The nonannular impact of the SAM is very similar to the local pressure anomaly of ENSO events and the surface anomalies mimic those of the ENSO triggered dipole anomalies. The enhanced westerlies of a positive SAM phase also enact a spin-up of the Weddell Gyre due to the "annular" impact of the SAM.

[10] The interference of the SAM and ENSO, particularly in the southeastern Pacific and over the Bellingshausen Sea region allows for complex modulations of impact [*Simmonds and King*, 2004; *Fogt et al.*, 2011]. *Stammerjohn et al.* [2008] have pointed out that when cold ENSO events are coincident with a positive SAM (and vice versa), they tend to reinforce each other's impacts on sea ice. More specifically, the associated pressure anomaly in the southeast Pacific is reinforced and shifted farther southeast, offering greater breadth of impact on the Weddell and Antarctic Peninsula regions. Figure 1 shows that this opposite-phasing of the two climate modes is present during much of the late 1990s and early 2000s when we have hydrographic observations, further motivating our study.

[11] Even though there is evidence that large-scale climate variability has impact on surface temperature and sea ice distributions in the Weddell Sea, whether these climate influences could be extended to the deep ocean remains unknown because of data scarcity. Perennial sea ice has made hydrographic observation difficult and as a result, all time series of hydrographic parameters to date have been too short to assess interannual variability relevant to external climate. Now, with an 8-year time series of bottom water potential temperature observed by deep-sea moorings in the northwest Weddell Sea [*Gordon et al.*, 2010], we have for the first time a record long enough to observe interannual variability. The goal of this study is to statistically relate the interannual variability observed in this record to large-scale polar and extrapolar climate variability (ENSO, SAM, ADP) and then to explain these relations through physical mechanisms of surface forcing, one related to dense water production and one related to dense water export.

2. Data

2.1. Mooring Data

[12] We use hydrographic data collected from a series of moorings south of the South Orkney Islands in the northwest Weddell Sea [*Gordon et al.*, 2010] (Figure 2). Collectively, they document the properties of bottom water at the northern limb of the Weddell Sea. The moorings were initially deployed in April 1999 and are redeployed every 2–3 years. Moored instruments document temperature,

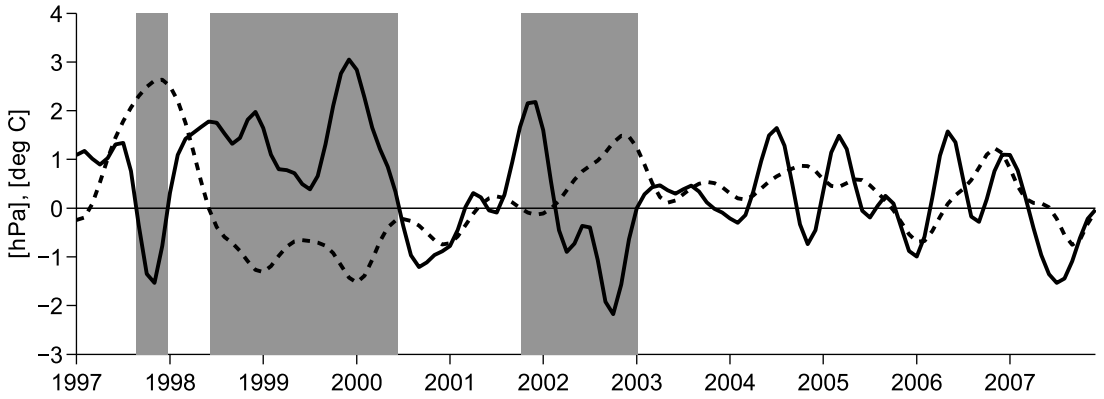

Figure 1. SAM (solid) and NINO3.4 (dashed) indices from 1997 through 2007. Out-of-phase occurrences of ENSO and SAM are in gray shading.

salinity, and velocities from near-bottom to 501 m above bottom at approximately 100 m intervals, with sampling rates varying from 7.5 to 30 min. The primary data used in this study are potential temperature records spanning from April 1999 through January 2007.

[13] Of particular interest is the lowest instrument at mooring M3, which at 4560 m depth represents the deepest and densest water of the Weddell Sea (Figure 3). There is a significant gap in the bottom-level potential temperature time series from 29 July 2004 through 7 March 2005, while the second-deepest instrument does not have this gap. Since the signal is vertically coherent, the record from the second-lowest instrument was substituted over this gap by subtracting the mean offset between the two instruments (−0.027°C). Potential temperature records from the bottom instrument at mooring M2 (depth 3096 m) overall demonstrate

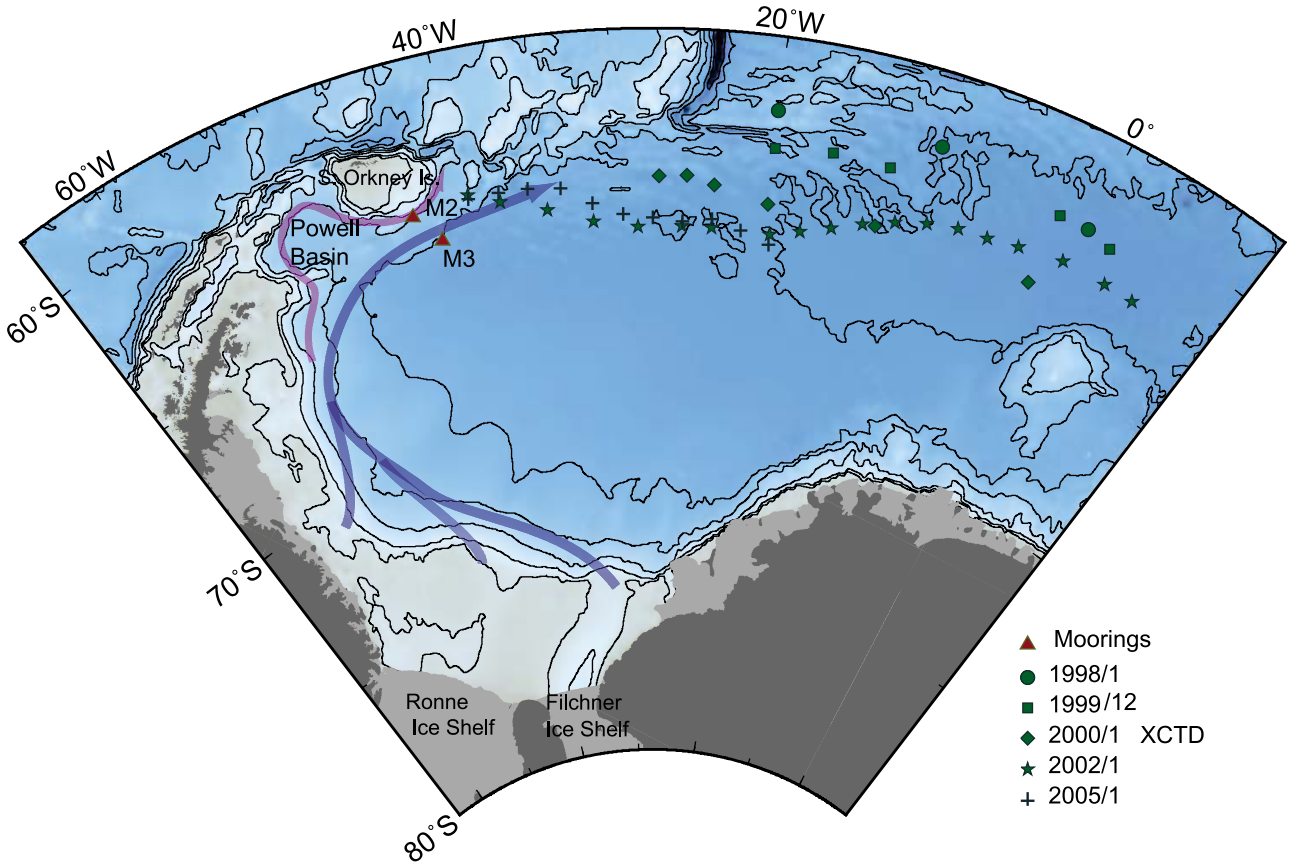

Figure 2. Locations of moorings M2 and M3 as well as the XCTD lines used in this study. Flow paths from potential source locations to the moorings are indicated, including the possible path around Powell Basin for the less dense water reaching M2. The permanent pycnocline base depths as calculated from the XCTD data are shown in Figure 9.

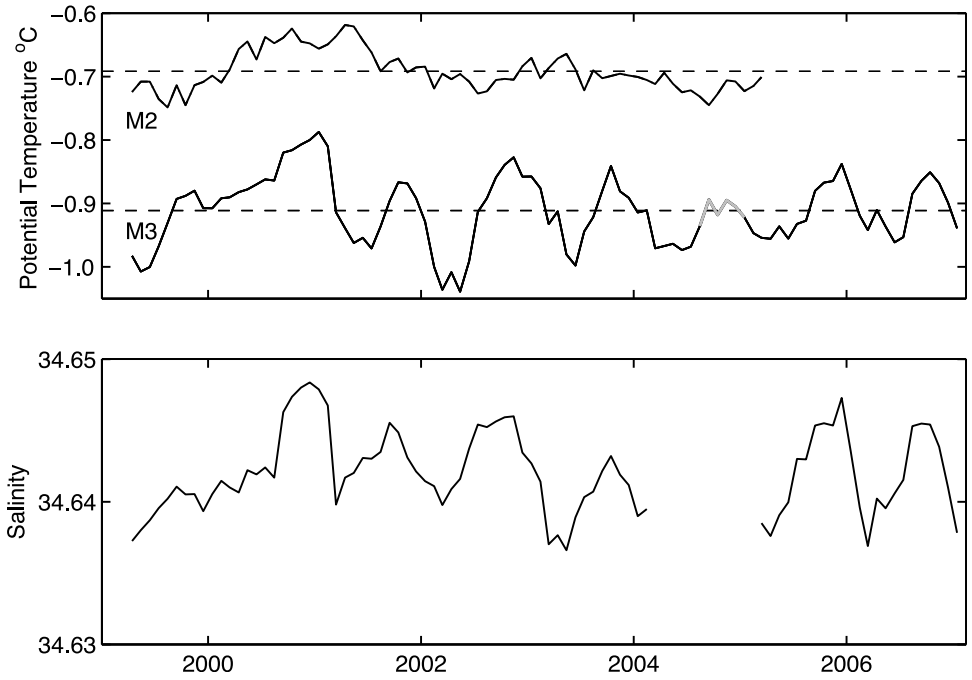

Figure 3. (top) Monthly potential temperature (θ°C) time series from bottommost instruments at moorings M2 and M3. The bottommost instruments are ~15 m off their respective mooring depths. The gray segment on the M3 temperature line marks the period where the record from the second-lowest instrument was substituted by subtracting the mean offset between the two instruments (−0.027°C). Also included are mean temperature values (dashed lines) at each mooring to help illustrate variability. (bottom) Monthly salinity time series from bottom instrument at mooring M3.

an identical interannual signal with a muted seasonal signal (Figure 3), so all analyses use data from both moorings. In addition to the potential temperature records we include some discussion of bottom salinity (Figure 3) and bottom speed at M3. There are more significant gaps in these records (explained by *Gordon et al.* [2010]), so we do not study statistics of these time series.

[14] The data are highly seasonal with cold pulses in austral winter. A detailed description of the seasonal variability is presented by *Gordon et al.* [2010]. While the structure of the temperatures is clearly vertically coherent, the increased vertical derivative of potential temperature during cold pulses indicates benthic intensification, suggesting export of dense water from the shelf occurs via gravity plumes. Velocities of approximately 12 cm/s at M3 suggest a transit time from likely shelf water source to mooring M3 of ~6 months. Of interest in this study is substantial interannual variability at M2 and M3 with anomalously cold pulses in 1999 and 2002 and an absence of a cold pulse in 2000, clearly evident in Figure 3. Data in year 2000 are warmer year-round, and the pulse in 2002 occurs earlier than usual.

[15] On the basis of θ-S profiles, the bulk of the water observed at M3 is believed to be sourced from shelf water in the southwestern Weddell, particularly the Ronne Ice Shelf area with some sourced farther north (Figure 2, middle and upper dark blue arrows, respectively) [*Gordon et al.*, 2010]. Though upon mixing Filchner Ice Shelf outflow derived bottom waters tend to become warmer and saltier and therefore fill the inner Weddell Sea as opposed to steering its outer rim [*Gordon*, 1998], we admit the possibility of their influence at M3 and therefore include the bottom dark blue arrow in Figure 2. M2 is believed to be sourced by shelf waters farther north [*Gordon et al.*, 2010], and this path is marked by the light blue arrow. The paths themselves are drawn on the basis of intense frontal mixing of shelf water and modified WDW at the slope and steering by the Coriolis force upon descent, thereby following topography.

[16] The fact that the potential temperature at M2 lacks seasonal variability and has a mean value near the WSBW/WSDW boundary of $\theta = -0.7$°C invites questions that parcels of water at M2 may not be derived from the same surface forcing that parcels at M3 respond to and that M2 may primarily be recording the variability of the ambient WSDW. We argue that the interannual variability observed at both moorings is forced by the same surface condition. The lack of a seasonal signal at M2 can be explained as follows. Parcels at M2 are likely derived from farther north [*Gordon et al.*, 2010] where the continental shelf is narrower and the slightly less dense shelf water over the western margin and northwest corner is less prone to seasonal forces. That is, the outflow is more constant in time since the shelf water is forced to run off a continuously narrowing shelf. Further, the sea ice over this region is much less variable seasonally with a climatological concentration near 100% year-round, limiting local atmospheric communication.

[17] A second interpretation is that while the water at M3 receives the direct impact of the seasonal injection of gravity currents, the shallower water of M2 sees this signal attenuated as the gravity current effects are mixed upward over a longer advective path. There is an offset of several months in timing of pulses between the two time series (max cross-correlation at 3 months offset), potentially due to

water traveling to M2 taking a longer path around the Powell Basin. Though an additional 3 months may not seem long enough to attenuate any seasonality since it is small in comparison to the ~6 month transit time to M3, which records a strong seasonal signal, there is reason to suspect strong vertical mixing occurs within the Powell Basin as suggested by data from the DOVETAIL program [*Muench et al.*, 2002]. The steep topography of the South Scotia Ridge generates a strong mixing intensity [*Heywood et al.*, 2002]. More specifically, dissipation of internal tide energy across the ridge from the conversion of barotropic to baroclinic tides can generate locally strong vertical mixing within the Powell Basin, even with weak stratification [*Muench et al.*, 2002; *Padman et al.*, 2006]. While lateral mixing with overlying WSDW along this longer advective path may contribute to a reduced seasonal signal, we argue that the properties of water at M2 are representative of WSBW by appealing to profiles of dissolved oxygen and potential temperature along the location of the moorings from the DOVETAIL program in 1997 [*Gordon et al.*, 2001] which show a clear WSBW core at both mooring sites.

2.2. Climate Indices

[18] A number of climate indices are used in this study. The NINO3.4 index is defined as the average sea surface temperature anomaly in the region bounded by 5°N to 5°S, from 170°W to 120°W, and is retrieved from the IRI/LDEO Climate Data Library. The SAM index is retrieved from the British Antarctic Survey, where they use the methodology outlined by *Marshall* [2003]. The definition is the same as the zonal mean definition proposed by *Gong and Wang* [1999], which is the difference in zonally averaged SLP anomalies between 65°S and 40°S, though to avoid using reanalysis data, 12 stations are used to calculate a proxy zonal mean sea level pressure at 65°S and 40°S. The ADP index is defined as the difference between DP1 and DP2 (DP1-DP2), where DP1 is the averaged sea ice concentration at the Pacific center of the ADP (130°–150°W and 60°–70°S) and DP2 is the averaged ice concentration at the Atlantic center (20°W–40°W and 55°–65°S).

2.3. Surface Variables

[19] The atmospheric data (sea level pressure, zonal and meridional winds, surface air temperature) are monthly means from NCEP-NCAR CDAS 1 data on a 2.5° latitude × 2.5° longitude grid. It is well-documented that, due to the limited number of observations in the southern high latitudes, NCEP-NCAR reanalysis data are not ideal [e.g., *Marshall and Harangozo*, 2000], especially before the satellite era; however, all data used are from after 1978. Sea ice concentrations, which are derived from space-born passive microwave measurements, are obtained from the National Snow and Ice Data Center. These satellite measurements have typical spatial resolution of 25 km and near-daily temporal resolution. Here we use monthly sea ice concentration derived by the bootstrap algorithm [*Comiso et al.*, 1997] and averaged them into a 0.25° latitude × 1° longitude grid. The ADP index described above was generated from these data.

2.4. XCTD Data

[20] To examine the spin up or down of the Weddell Gyre, sections of expendable conductivity, temperature, depth (XCTD) lines across approximately 60°S are used in this study. These data were taken from Chinese vessel M/V XueLong under U.S./Chinese ship-of-opportunity sampling programs [*Yuan et al.*, 2004] in the summers 1998, 2000, 2002, and 2005 (Figure 2). All XCTD profiles went through a careful quality control procedure guided by *Bailey et al.* [1993]. The manufacturer's specified accuracy of XCTD is about +/− 0.02°C for temperature and +/− 0.07 ppt for salinity, both of which are adequate for the purpose of identifying the base of the permanent pycnocline. These repeat sections were taken in the same season with relatively consistent locations, making the data set very valuable to assess interannual variability in the upper ocean's response to climate forcing.

3. Results

3.1. Relation to Large-Scale Climate Variability

[21] Our first approach to assess the relationship between the potential temperature variability at moorings M2 and M3 and climate forcing was through linear correlations between the time series of temperature anomalies at each mooring and the three climate indices. All linear correlations considered 24 months of lead/lag relationships, allowing for assessment of a broad range of surface forcings, teleconnections, and transit times. The method of lagged correlation is described in section A1. We filtered all time series with a Butterworth filter with width of 6 months prior to correlation calculation to reduce subannual variability. We evaluated correlation significance with a bootstrapping method described in section A2.

[22] Correlations peak with indices leading on the order of 14–20 months. Maximum correlations with their significance values are presented in Table 1 with their corresponding lag time, with both time series filtered by 6 months. Table 1 also reports a significance value for the lag time (see section A2). Correlations as a function of lag time are shown in Figure 4. While we have very good confidence in the lag time of maximum |r|, the distributions of high |r| values across adjacent lag times are broad. This is due in part to the memory of the time series and also to any complex sequence of events linking large-scale anomalies to local forcings and then to the deep ocean (and the time-variant nature of these events).

[23] The difference in response to NINO3.4 between M2 and M3 may be in part due to the reduced seasonal signal at M2. The correlations of temperature anomalies at M2 and M3 with NINO3.4 index and with ADP index over different leads reveal one peak that gradually dissipates over adjacent leads. This, combined with the fact that $|r_{ADP}| \geq |r_{NINO3.4}|$ for M3 (though they are approximately equal for M2), suggests that ENSO's impact on bottom water temperature variability is realized through the development of ADP, which happens during 3 to 6 months after the peaks of ENSO events [*Yuan*, 2004]. On the other hand, the correlations of temperature anomalies at M2 and M3 with SAM index reveal a second peak of opposite sign (though less significant with all $p > 0.1$) at approximately 1–6 months lead time. This could imply bottom water production or export responds to the SAM at various time scales.

3.2. Coherent Regional Surface Forcing

[24] The statistically significant correlations with the climate indices and the complex nature of modulation between

Table 1. Maximum Correlation Coefficients Between Potential Temperature Anomalies and Climate Indices[a]

	θ Anomaly at M3		θ Anomaly at M2	
	r	Lead	r	Lead
NINO3.4	−0.41, 89%	21, 99%	−0.73, 97%	21, 99%
SAM	+0.38, 98%	14, 99%	+0.54, 99%	20, 99%
ADP	+0.48, 99%	15, 99%	+0.71, 99%	17, 98%

[a]Here r is the linear correlation coefficient between given index and potential temperature time series. Significance levels are reported next to r value and lead value. The methods of lagged correlation and significance testing are described in sections A1 and A2, respectively. Lead time corresponds to number of months the index leads the temperature time series.

ENSO and SAM in the Antarctic Peninsula region suggest the need to capture coherent surface forcing patterns that are combined results from different influencing sources. To do so, we computed a multivariate empirical orthogonal function (MEOF) analysis using surface forcing variables of sea level pressure (SLP), surface air temperature (SAT), zonal and meridional winds, and sea ice concentration (SIC). For all fields, anomalies were calculated about a climatology of January 1997 to December 2006 and were detrended, standardized, and smoothed by a Butterworth filter with filter width of 6 months.

[25] The spatial pattern of the first MEOF mode is presented in Figure 5. The first mode is clearly indicative of surface anomalies (SLP and zonal winds) associated with the SAM [*Thompson and Wallace*, 2000; *Lefebvre et al.*, 2004; *Simmonds and King*, 2004] and classical ADP patterns in SAT, meridional winds, and sea ice [*Yuan*, 2004]. The SLP field demonstrates the high-pressure anomalies at 40°S and low anomalies at 65°S associated with enhanced zonal winds, a signature of positive phase SAM. The zonal asymmetry of SAM is seen, with a clear dent in the SLP pattern near 90°W, 60°S, which is coincident with the coherent ENSO/Pacific South America (PSA) pressure anomaly over the Bellingshausen Sea. This pressure anomaly results in coherent ADP anomalies in meridional wind, SAT, and sea ice concentration fields [*Yuan*, 2004]. The anomalous meridional winds associated with the anomalous pressure center advect warm oceanic air south in the Pacific sector and cold continental air north in the Atlantic sector, resulting in temperature anomalies and thermodynamically driven outer ice extent anomalies. This anomalous wind pattern also affects sea ice concentration dynamically, resulting in a north/south contrast with inner ice pack variability related to dynamical packing (potentially thickening) near the coast in the Weddell Sea and vice versa in the Pacific sector.

[26] Mode two (not shown) seems to be a transition mode, dominated by Western Hemisphere wave-3 patterns in SAT, zonal wind, meridional wind, and sea ice concentration. The wave-3 is a well-established climate pattern in the Southern Hemisphere, supposedly caused by the land/ocean distribution [*Raphael*, 2004]. It acts to advance the ice edge at synoptic time scales and provides preferred locations for cyclogenesis in the open ocean north of the ice cover [*Yuan et al.*, 1999]. It demonstrates a significant relation to local ice cover [*Raphael*, 2007; *Yuan and Li*, 2008].

[27] The variance explained by mode one (22%) is comparable to findings for the first mode of SLP anomalies attributed to SAM in other studies [e.g., *Simmonds and King*, 2004]. Figure 6 shows the leading principal component and its correlations with the temperature anomalies at M2 and M3. The phasing of the time series is similar to that of the SAM index and it correlates significantly with WSBW potential temperature anomalies on the same lead scales as did the SAM index, though with higher correlation coefficient values (on the order of 0.5–0.6) when the correlations are significant. As with correlations involving the SAM index, opposite sign, marginally significant, and weaker correlations are present with the principal component leading by a shorter 1–6 month lead.

[28] Computing MEOF analyses with other combinations of variables always yields essentially identical spatial modes, though with slightly varying variance explained and peak correlation leads for each mode. The variability in variance explained is likely due to inherent lead-lag times in the ice-atmosphere system, causing a bleeding between fields. For example, the highest variance explained was obtained when considering only dynamical variables (32% by mode 1 SLP and winds), omitting the time necessary for sea ice concentration (and to a lesser extent, SAT) to respond to advected air.

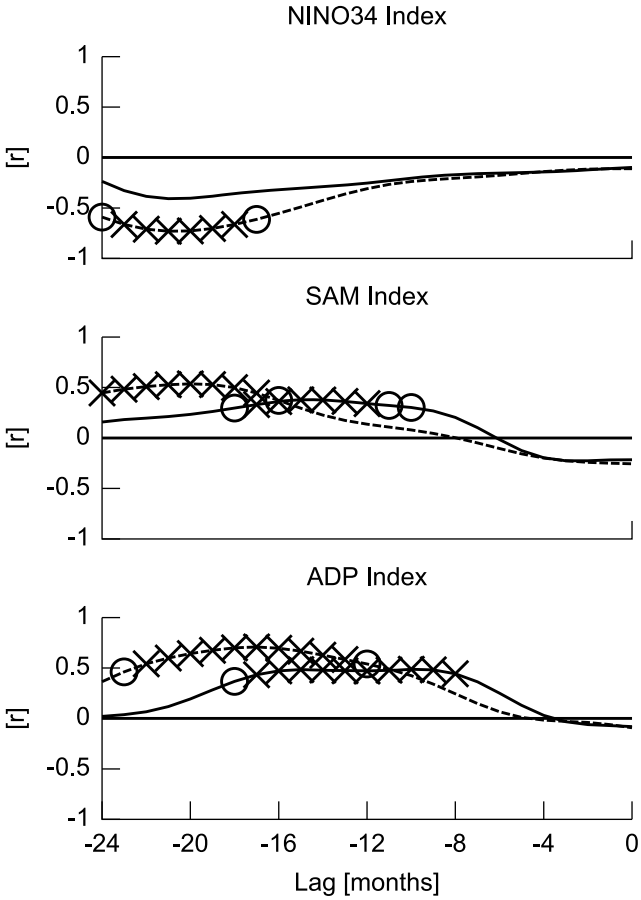

Figure 4. Correlations between temperature time series (M2 dashed, M3 solid) and climate indices, plotted as a function of lag time (number of months the climate indices lag the temperature time series). Correlations significant above 90% are marked as circles and correlations significant above 95% are marked as crosses.

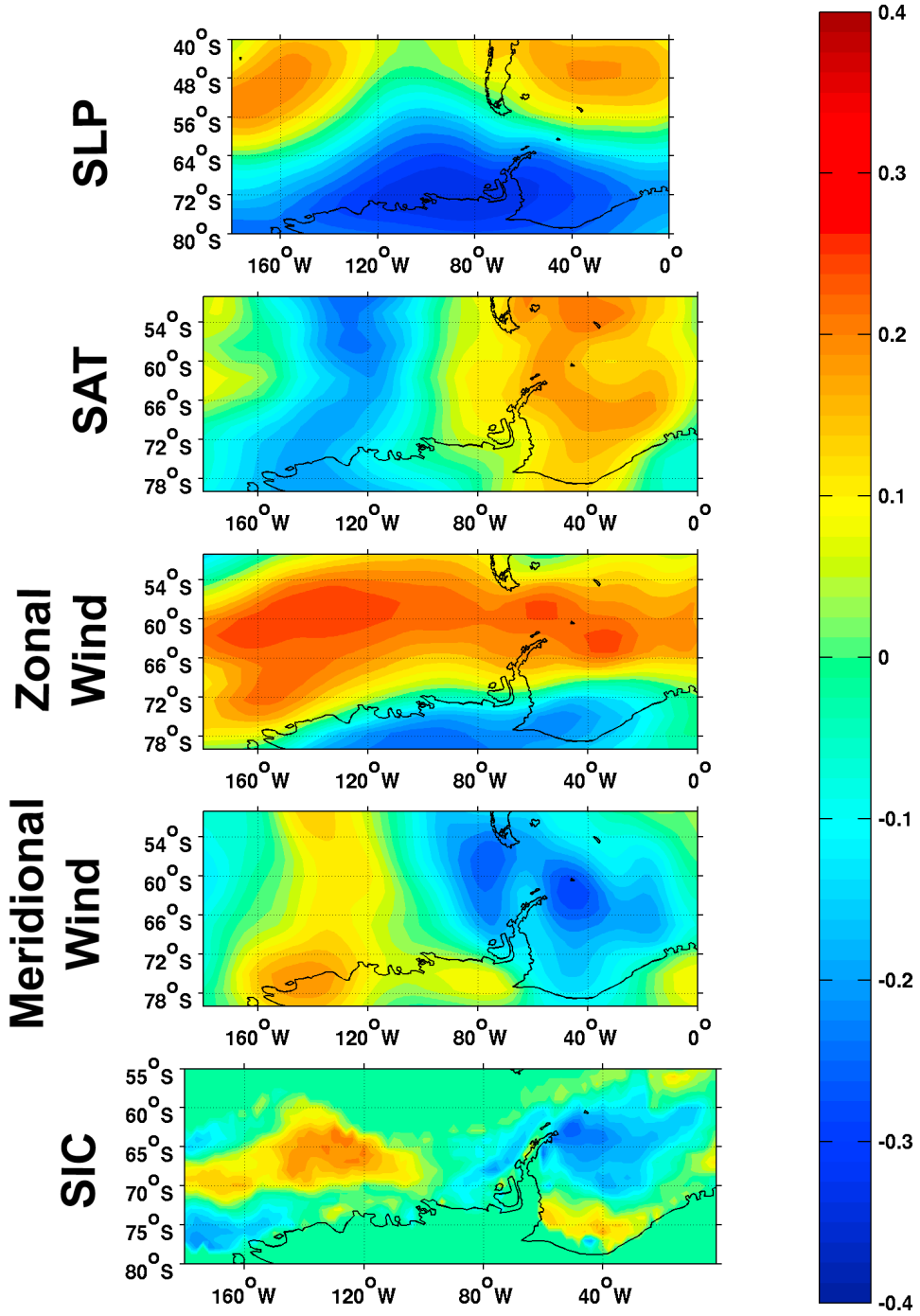

Figure 5. Spatial patterns of the first mode of MEOF analysis. First mode resembles +SAM and PSA pattern.

3.3. Local Winds and Sea Ice Fields

[29] The spatial patterns of the leading MEOF mode and its strong correlations with WSBW temperature anomalies invite physical interpretations at the local scale. First, we examine relationships with meridional winds and sea ice concentrations over the continental shelf. With a residence time of ~5 years [*Mensch et al.*, 1996], the shelf water that escapes each austral summer is a blend of dense water types formed from previous winters. The residence time is largely due to a rather sluggish circulation in the vertical plane where shelf salinity increases to the west, leading to a geostrophic vertical circulation [*Gill*, 1973]. Nevertheless, contributions from the immediately preceding winter can be strong in the case of anomalous surface conditions via either greatly increasing or failing to replenish supply. Bearing this in mind, in combination with the estimated transit time of ~6 months from likely shelf water source to mooring M3, anomalous ice conditions 4–5 seasons before corresponding

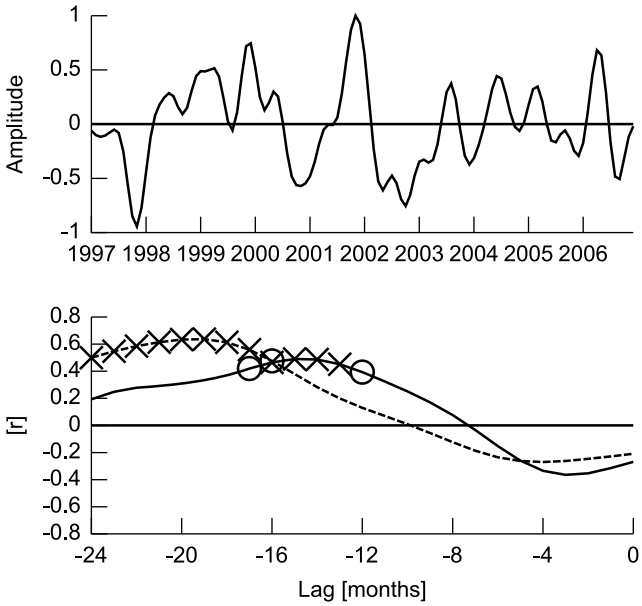

Figure 6. (top) The principal component of the leading mode from MEOF analysis shown in Figure 5. (bottom) Correlation of the principal component with potential temperature anomalies (M2 dashed, M3 solid). Horizontal axis indicates number of months the principal component lags the temperature time series. Correlations significant above 90% are marked as circles and correlations significant above 95% are marked as crosses.

observations at the moorings should be relevant. As such, relationships between potential temperature and both sea ice concentration anomalies and meridional wind anomalies were assessed through linear correlations. This is not to say that the properties (θ-S) of the shelf water formed in a given year will necessarily be reflected in the immediately following export but rather that a greater formation of dense shelf water in a given year will yield a greater supply of source water on the shelf, and therefore a stronger contribution from the "cold end-member" along the mixing line for WSBW, resulting in a colder product.

[30] Figure 7 shows correlation coefficients between sea ice concentration anomalies and potential temperature anomalies at the moorings. Of primary interest is the north/south contrast in correlations, separated by the shelf slope. The patterns suggest that increased (decreased) summer sea ice concentration over the continental shelf the summer before export corresponds to a warmer (colder) pulse in the deep ocean later or less (more) dense shelf water exported. Increased sea ice concentration over the shelf and reduced sea ice extent is consistent with strong southward wind anomalies in the western Weddell, mechanically preventing advection of sea ice and thermodynamically hindering the formation of new sea ice the following winter, consistent with the anomalous winds of both positive SAM and La Niña [*Yuan*, 2004; *Lefebvre and Goosse*, 2005]. Some characteristic correlation values are presented in Table 2.

3.4. Wind Stress Curl and Upper Ocean Structure

[31] The WSBW temperature could also be affected by the volume of dense water exported from the shelf each year. As mentioned before, the degree of baroclinicity in the Weddell Gyre is a factor influencing the escape of dense water and this in turn is related to the wind stress above the gyre [*Jullion et al.*, 2010]. To evaluate cyclonic forcing, we calculated the wind stress using the algorithm of *Smith* [1988], modified to allow for zonal and meridional components, and then computed the curl of this vector field. We then calculated curl anomalies with the climatology from January 1997 to December 2006 and spatially averaged them to obtain a single time series (Figure 8), as done by *Gordon et al.* [2010]. The averaging domain (marked in Figure 8) includes the area bounded by the continental slope in the central Weddell Sea west of the Prime Meridian. While correlations of this time series with the temperature anomalies at M2 and M3 are low (best r of 0.25 at the confidence level of 73%), they are qualitatively reasonable. Approximately 6 months before the coldest anomaly of 2002, the wind stress curl anomaly reaches its most negative (cyclonic) value in the entire period of 1996–2008. Further, the wind stress curl anomaly is negative for a prolonged period before 1999's cold pulse and is largely positive throughout 1999 and 2002, preceding the lack of a cold pulse in 2000 and the warm period of late 2002 to early 2003, respectively. The largest increases in cyclonic forcing seem to coincide with sudden shifts in the phase of the SAM from negative to positive (Figures 1 and 8).

[32] To demonstrate the spin up or down of the gyre, we examine the variability of the permanent pynocline base (PPB) depth as calculated from the XCTD data (stations shown in Figure 2). The PPB depth is identified from density profiles. Each density profile was visually inspected for the selection of key points because, as these are summertime observations, we needed to distinguish between the seasonal and permanent pycnocline. Then, we calculated the PPB depth as the depth of the maximum value of $|\nabla^2\rho|$, where ρ is density [*Martinson and Iannuzzi*, 1998]. Figure 9 shows the PPB depth of these repeat sections in comparison with historical data. The samplings west of approximately 15–20°W correspond to the gyre rim, whereas data east of this divide are more indicative of the gyre's center. As such, the PPB depth relative to the mean in the central gyre can serve as a proxy for degree of baroclinicity within the gyre.

[33] The PPB depths are in good agreement with the wind stress curl observations. Between 0° and 20°W where the data fit within the center of the Weddell Gyre, the mean PPB depth in January 1998 when there was enhanced annual mean cyclonic forcing is shallower than in December 1999 when there was diminished annual mean cyclonic forcing. In the same region, the mean PPB depth for January 2002 when there was enhanced annual mean cyclonic forcing is shallower than the historical mean, and the mean PPB depth for January 2000 when there was diminished annual mean cyclonic forcing is deeper than the historical mean. West of 20°W where the data more accurately correspond to the gyre's outer rim, the mean PPB depth in January 2002 is deeper than the historical mean, a clear signature of gyre spin up associated with strong cyclonicity in winds.

[34] A few words should be said about the Weddell Gyre to express the shortcomings of our method. The transport of the gyre is primarily barotropic [*Klatt et al.*, 2005]. West of the Prime Meridian, the gyre is flanked by the Weddell

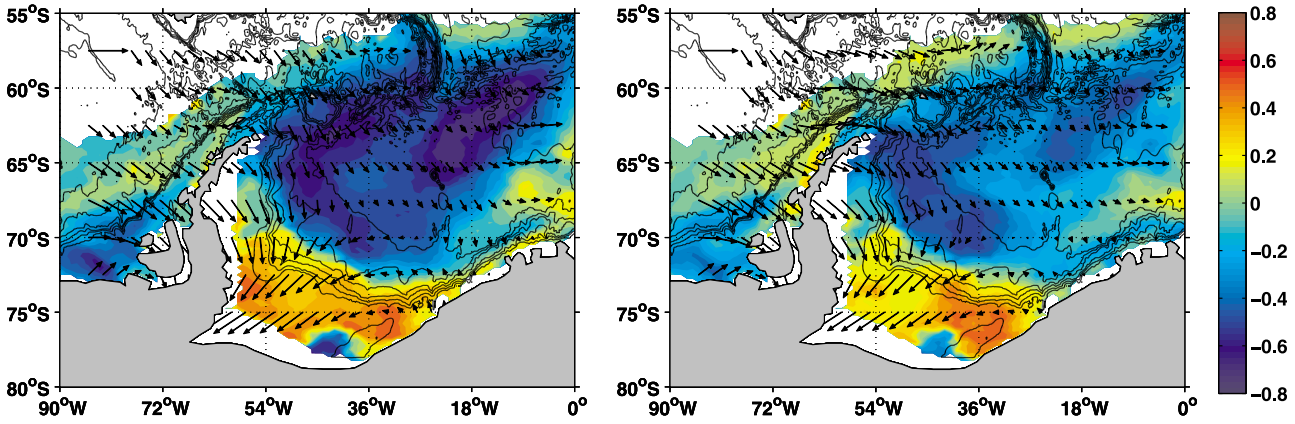

Figure 7. Correlation coefficients between sea ice concentration anomaly as well as wind anomaly and temperature anomalies at (left) M2 and (right) M3. Sea ice and winds lead M2 by 17 months and M3 by 14 months. Sea ice correlations are color-coded while wind correlations are presented as vectors whose x component is r_{zonal} and y-component is $r_{meridional}$. Vector of length 1 is shown in top left corners.

Front to the north and the Antarctic Coastal Current to the south. Only the coastal current demonstrates clear seasonal variability, which is also primarily barotropic. While the baroclinic component of this current is small, it can be important in that this component of the gyre forms the fresh v-shaped front (and its outer limb contains the WDW) involved in the shelf-slope mixing processes [*Gill*, 1973]. It is found that the Sverdrup transport (mean wind stress curl) explains 30% of this baroclinic variability [*Nuñez-Riboni and Fahrbach*, 2009]. The idea that a mean wind curl can relate to the spin up or down of the Weddell Gyre implies a gyre that is quasi-fixed in space with one mode of variability, though we attempt to be as flexible as possible with this constraint by carefully defining our averaging domain. For example, because the gyre demonstrates a "double cell" structure centered about the Prime Meridian [*Beckmann et al.*, 1999, and references therein], we defined our eastern bound to be west of this divide. Further, a meridional displacement of the west wind (and corresponding currents) has been observed, with west winds low in the north and east winds high in the south through the early 1990s and mid 2000s with the opposite pattern in the time between

Table 2. Correlation Coefficients Between Surface Anomalies and Potential Temperature Anomalies[a]

	θ Anomaly at M3		θ Anomaly at M2	
	r	Lead	r	Lead
Mean meridional wind anomaly	−0.64, 99%	13, 99%	−0.71, 99%	16, 99%
Sea ice concentration anomaly (56°W, 73.25°S)	+0.52, 99%	14, 99%	+0.53, 99%	17, 98%
Sea ice concentration anomaly (33°W, 76.25°S)	+0.40, 94%	16, 99%	+0.52, 99%	18, 98%

[a]Here r is the linear correlation coefficient between given surface anomaly time series and potential temperature time series. The methods of lagged correlation and significance testing are described in sections A1 and A2, respectively. Lead time corresponds to number of months the surface anomaly time series leads the temperature time series. The mean meridional wind anomaly is averaged over the region 65°W–45°W, 77.5°S–67.5°S.

(E. Fahrbach et al., Warming of deep and abyssal water masses along the Greenwich meridian on decadal time scales: The Weddell gyre as a heat buffer, submitted to *Deep Sea Research, Part II*, 2011). So, our northern and southern bounds cover the full extent of the central latitude bands.

4. Discussion

[35] As shown above, we propose that there are two mechanisms that could produce temperature fluctuations in the deep ocean. First is the process affecting the volume of dense shelf water available, operating on 14–20 month scales. Second is the process affecting the export of dense shelf water, operating on 1–6 month scales. While first mentioned by *Gordon et al.* [2010], here we discuss these processes in more detail and explain their relation to large-scale climate modes.

[36] The two mechanisms we consider are those that we believe should have the most impact on the variability of WSBW properties. In theory, the observed variability at the moorings could be related to a shift in the current's core; variable shelf water source, properties, or export; variable amount of modified WDW in mixture or properties of injected WDW; variable air-sea heat fluxes during low ice cover; or variable circulation patterns of water on the shelf.

[37] We do not believe that the variability recorded at the moorings is due to a shift in the cold core of the current given the moorings' locations at steep topographic escarpments, which serve to guide the bottom current and create a fixed WSBW stream [*Gordon et al.*, 2010]. While we cannot test for a shift in source without in situ measurements on the shelf, the fact that M2 and M3 demonstrate the same interannual signal while being sourced from different regions suggests that source location is probably not of primary importance. We cannot completely refute the possibility of variable WDW properties or amount of modified WDW injected being significant as the thermohaline properties of WDW have in some observations been directly related to those in WSBW [*Fahrbach et al.*, 1995]. Instead we can only emphasize our measurements are strictly of bottom-most WSBW directly affected by gravity plumes less susceptible to vertical mixing. We assume the shelf circula-

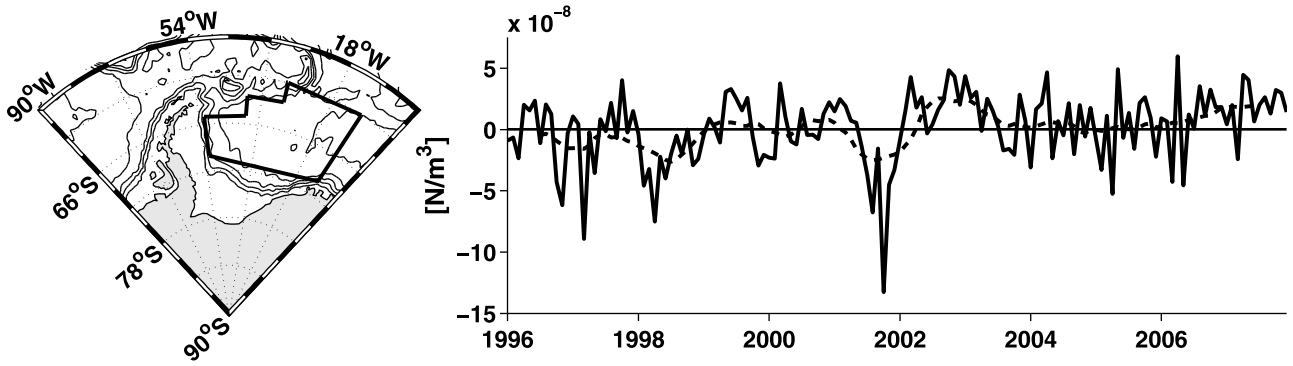

Figure 8. Time series of mean wind stress curl anomaly averaged over the Weddell Sea, with averaging domain indicated in the map to the left. Important to note are the strongly negative values in late 2001 as well as the subtly positive values in 1999.

tion is approximately constant given its slow nature. Last, atmospheric heating should not have a significant effect on shelf water properties as the effect is limited to the upper 30 m, a cap which is overcome rapidly by late fall or early winter cooling [*Martinson*, 1990; *Martinson and Iannuzzi*, 2003].

[38] The range of salinity we observe at the moorings is within the range of the net sea ice effect on bottom water salinities which is about 0.15–0.20 difference between source/product waters [*Toggweiler and Samuels*, 1995]. Given this and the presence of gravity current injection, we suspect that the two processes affecting the production and export of dense water should be the most important in determining WSBW thermohaline properties.

4.1. Mechanism I: Dense Shelf Water Production

[39] The dense water production is directly related to the brine release from sea ice formation. The anomalous sea ice concentration patterns in the southwestern Weddell Sea appear strongly related to mean meridional wind anomalies over the western Weddell Sea (Figure 10) as suggested by *Gordon et al.* [2010]. Sea ice concentration anomalies over the continental shelf can be negative only in the austral summer because by winter the nearshore sea ice pack is mostly 100% covered. Our results show that winter cold pulses in WSBW are related to sea ice and wind anomalies in summer with a lead time of 14–20 months. In summer, an enhanced northward meridional wind advects more ice and surface freshwater, increasing leads and coastal polynyas. Then, come winter, the larger open area allows more sea ice formation, producing more dense shelf water. The very strong El Niño of 1997–1998 demonstrates this impact quite well, resulting in the opening of the Ronne Polynya with a greatly reduced sea ice cover throughout the summer and into the fall. The very strong anomalous northward winds associated with this ENSO event were responsible for opening the Ronne Polynya and created an anomalously large glut of HSSW [*Ackley et al.*, 2001; *Nicholls and Østerhus*, 2004]. This would, consequently, relate to 1999's cold anomaly in WSBW.

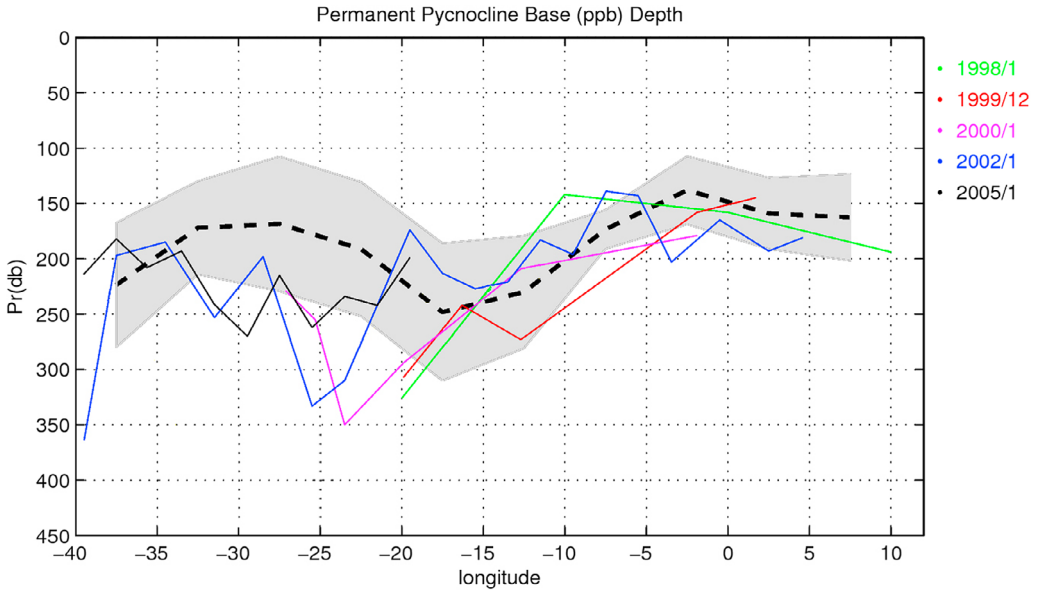

Figure 9. Permanent pycnocline base depth as calculated from XCTD data. Dashed line is historical mean with gray shading indicating one standard deviation. Values for each year are color-coded and do not necessarily span all longitudes. For a corresponding map of locations used, see Figure 2.

[40] Likewise, a weakened northward meridional wind will advect less ice and increase sea ice concentration over the continental shelf, which reduces freezing and thus dense shelf water formation in winter. A modeling study by *Timmermann et al.* [2002] made the link between meridional wind, sea ice concentration, and HSSW. They showed that after a period of sustained southward winds (that is, the anomaly is large enough so that the mean winds reverse direction), the volume of HSSW decreased, ultimately to zero. The mean meridional wind over the western Weddell Sea was indeed due southward for the entirety of 1999 (Figure 11), completely reversing the direction from the climatological mean, which should result in a reduction in dense shelf water. This would explain the absence of a cold pulse of WSBW in 2000. While other warm potential temperature anomalies at M2 and M3 correspond to increased sea ice concentration over the continental shelf and negative meridional wind anomalies, no other event has the mean meridional wind in our averaging region of the western Weddell southward for the period of a year.

[41] Salinity observations support the validity of this mechanism. A θ-S diagram shows that salinity during the cold pulses reveals a fan-like appearance with 2001 and 2002 being notably saltier than other events [*Gordon et al.*, 2010]. This trait was originally attributed to source variability [*Gordon et al.*, 2010] though we offer an alternate interpretation. A time series of salinity reveals that salinity during cold pulses increases from a low in 1999 to a high in 2002 before being notably lower again in 2003 (Figure 3). The increase from 1999 to 2002 appears near linear. The trend line for this portion of the time series has a slope about two orders of magnitude higher than that of observed WDW salinification over the 1990s [*Fahrbach et al.*, 2004]. Instead, we refer to the tremendous amount of HSSW produced in early 1998. The prolonged ice-free region near the Ronne Ice Shelf and the very strong and directionally constant winds may have fostered a more vigorous shelf circulation. As such, while more HSSW was formed with the winter freeze, the primary pulse would likely be rather fresh as water parcels would spend less time underneath the polynya collecting salt [*Grumbine*, 1991]. This would yield a cold but fresh pulse in 1999. As the brines incorporate into the shelf water, their influence on subsequent exports would increase, yielding increasingly salty water through 2002. The reversion to low salinity in 2003 suggests that the effect of this anomaly originating in early 1998 was finished by the late 2001 export, fitting rather well with Gill's estimate of 3.5 years required for complete exchange of shelf water, estimated using a salinity budget [*Gill*, 1973].

[42] The prevailing circulation of sea ice within the gyre includes a clockwise circulation with old ice arriving from the east and packing in the southwest before circulating north. For more shelf water production, it is important that the summer ice response over the southwestern shelf be driven by cold northward winds and not local melt. This is probably not a problem as temperatures are subfreezing year-round and upwelling of WDW has little influence on polynya formation [*Ackley et al.*, 2001]. Similarly, for less dense water production, that effect is enhanced if warm southward wind anomalies increase summer ice concentration over the shelf. To maximize the efficacy of the mechanism, the enhanced (weakened) summer wind may continue into winter to maintain (hinder) a polynya at the ice shelf beyond the initial freeze (or lack thereof).

4.2. Mechanism II: Shelf Water Export

[43] An enhancement of cyclonic wind-forcing corresponds to a more vigorous gyre circulation through baroclinic adjustment, which favors export of dense water and can be revealed by a doming of isopycnals in the central gyre and deeper isopynals at the gyre's rim [*Meredith et al.*, 2008; *Jullion et al.*, 2010]. As stated above, the correlations between mean wind stress curl anomaly and potential temperature anomalies at the moorings are weak. However, the lead time of 1–6 months and the clear qualitative fit between the largest anomalies in each time series are suggestive [*Gordon et al.*, 2010]. For one, the lag time is physically realistic and sits well with the proposed amount of time required for the gyre to respond to wind-forcing [*Jullion et al.*, 2010]. Second, the lead time matches the lead time of the weaker secondary correlations of the SAM index (and first principal component of MEOF analysis) with potential temperature anomalies at the moorings.

[44] The link between wind stress curl and PPB depth suggests that the mechanism of spinning the Weddell Gyre up or down in response to cyclonic forcing is indeed realistic. Moreover, the fact that the mean wind stress curl anomaly is consistent with the phase of the SAM other than in years of strong and unfavorable ENSO related anomalies (for example, La Niña event in calendar year 1999) suggests that the SAM influences the ocean-ice-atmosphere system at different time scales. A baroclinic adjustment of the Weddell Gyre to wind forcing is attributed to ENSO by *Martinson and Iannuzzi* [2003] and to the SAM by *Jullion et al.* [2010]. Our lagged correlations (Figure 4) favor the idea that the SAM has more of an impact on a shorter term relevant for spin-up.

[45] One might expect that an increased export of dense water toward the moorings would result in a higher speed in the bottom layer accompanied by a stronger vertical shear ($d|\mathbf{u}|/dz$). Figure 12 shows that bottom temperature decreases with the increase in both speed and shear in the bottom layer, as expected. Even with large scatter, the approximate linear relationship supports a fast flow associated with increased export. We are limited to a crude estimate of the shear (computed from two instruments separated vertically by 501 m). This may not be sufficient for accurate vertical resolution, especially for vigorous plumes (which may be thicker), as demonstrated by the notable deviation from the trend at the coldest temperature.

4.3. Specific Roles of SAM and ENSO in Driving Surface Forcings

[46] We begin this section with the presentation and interpretation of a linear statistical model designed to link the indices to the relevant surface variables and then link these variables to the observed bottom water variability. The model is an ensemble of multiple linear regressions. On the basis of proper lag times (those of maximum correlations), the three indices (NINO3.4, SAM, and ADP) were fit to shelf-averaged meridional wind; sea ice concentration at 56°W, 73.25°S; and gyre-averaged wind stress curl in three separate multiple linear regressions. Then, the indices were run through each of these models to create three time series of

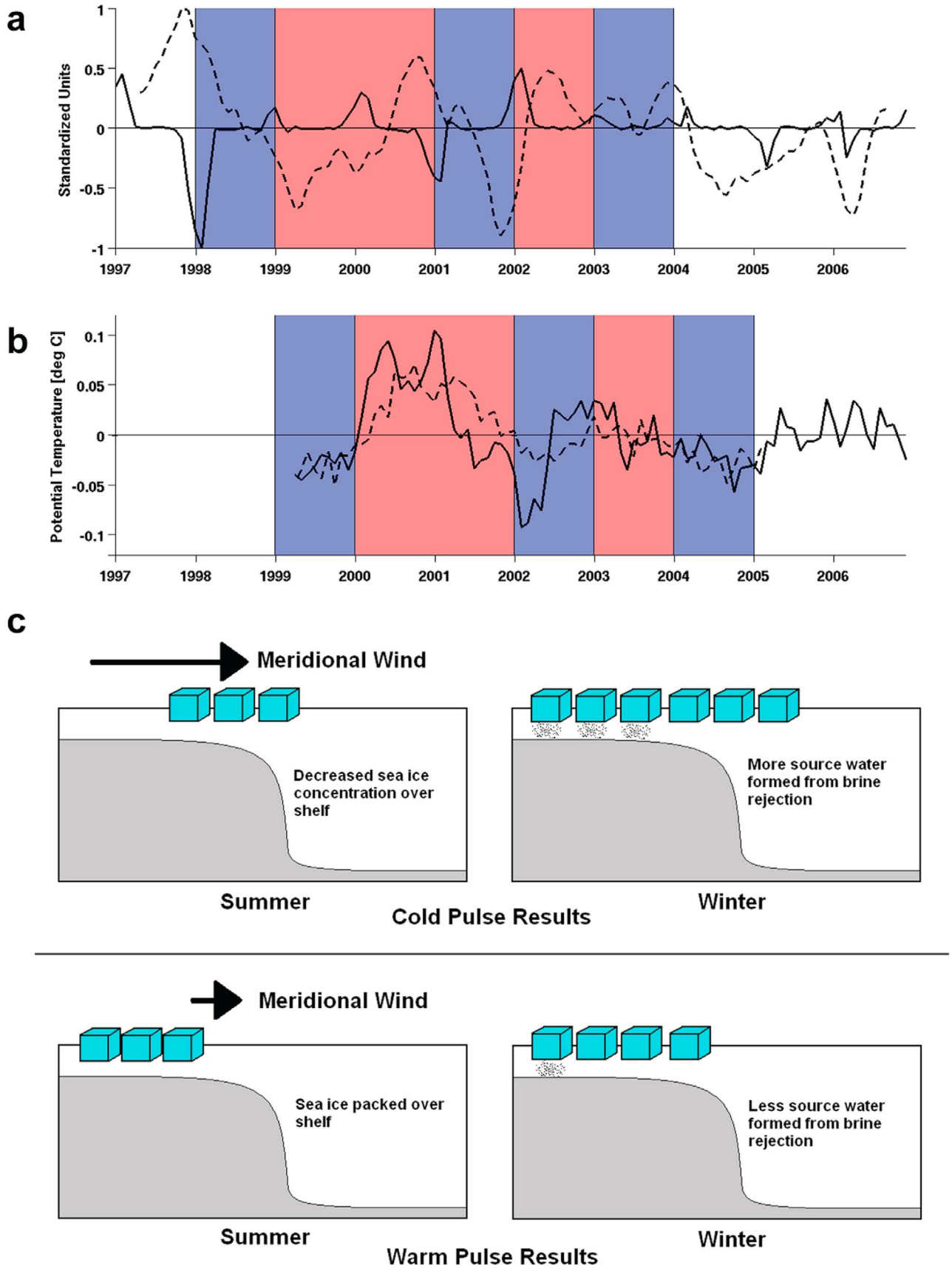
a
Standardized Units
1
0.5
0
-0.5
-1
1997
1998
1999
2000
2001
2002
2003
2004
2005
2006
b
Potential Temperature [deg C]
0.1
0.05
0
-0.05
-0.1
1997
1998
1999
2000
2001
2002
2003
2004
2005
2006
c
Meridional Wind
Decreased sea ice concentration over shelf
More source water formed from brine rejection
Summer
Winter
Cold Pulse Results
Meridional Wind
Sea ice packed over shelf
Less source water formed from brine rejection
Summer
Winter
Warm Pulse Results

Figure 10

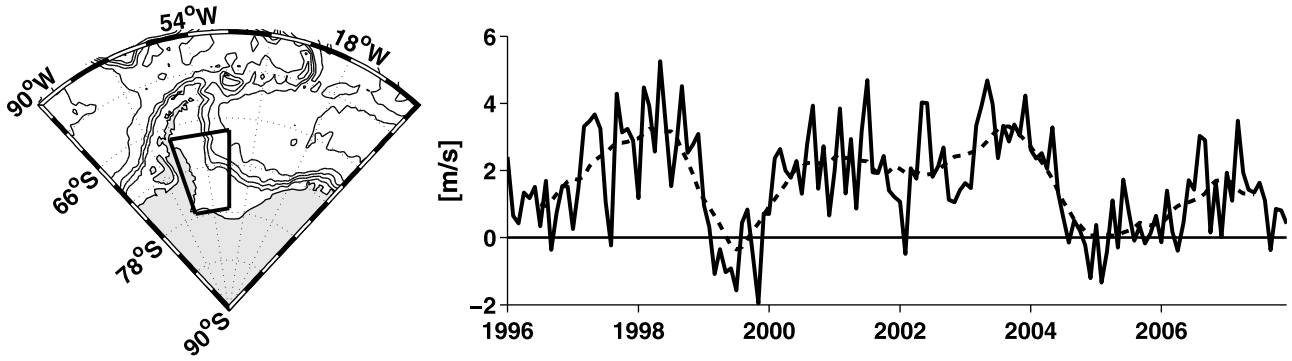

Figure 11. Time series of spatially averaged meridional wind values (solid line) and 12 month running mean (dashed line). The averaging domain is indicated in the map to the left. This shows the reversal of the climatological winds in 1999.

"predicted" mean meridional wind, sea ice concentration, and mean wind stress curl. Finally, these predicted time series were fit to the M3 temperature time series in a final multiple linear regression at lag times of maximum correlation which are consistent with those described in mechanisms I and II (Figure 13). Given the multicolinearity within the indices and the short nature of the time series, it is unrealistic to predict the bottom temperature or assess the significance of these regressions.

[47] The result seems to capture the main interannual variability of the M3 temperature time series when climate forcing is large (1999–2004). We believe that this implies a degree of predictability from the climate indices. More specifically, it is our belief that the correlations with the indices are indicative of causality between ENSO and SAM related anomalies and WSBW properties.

[48] In section 4.1 we have shown that the physics implied by the spatial pattern of correlations in Figure 7 are consistent with Mechanism I. What remains to be shown is whether these patterns are related to large-scale climate modes. The wind correlations demonstrate a strong meridional component and are centered about a pressure anomaly in the eastern Pacific. The ice response suggests a thermodynamic component (reduced extent due to southward advection of warm air) and a dynamic component (increased shelf concentration due to reduced northward advection of ice). These patterns are indicative of the ADP [*Yuan and Martinson*, 2001; *Yuan*, 2004].

[49] We believe the primary role of the ENSO is in the generation of these ADP anomalies which drive Mechanism I. The "hierarchy" of correlation coefficients with bottom temperature and an assessment of the their respective lead times supports this. First, it is true that $|r_{\text{merid wind}}| \geq |r_{\text{ADP}}| \geq |r_{\text{NINO34}}|$ at M3 (though these values are approximately equal at M2) (Tables 1 and 2). Second, the lead time for NINO3.4 with bottom potential temperatures is approximately 3–5 months longer than that for ADP with bottom potential temperatures while the lead times for both sea ice and meridional wind with bottom potential temperatures are approximately equal to those of ADP with bottom water potential temperatures. *Yuan* [2004] shows that ADP anomalies begin to manifest about a season after climate forcing matures in the Tropical Pacific, consistent with this value.

[50] Our results suggest that a positive (negative) phase SAM corresponds to a warmer (colder) temperature anomaly 14–20 months later. The main contribution of SAM at this time lead comes from its nonannular component, and it is well-documented that this nonannular component can induce a very similar dipole pattern of anomalies [*Lefebvre et al.*, 2004; *Holland et al.*, 2005]. However, our record is dominated by periods where SAM is out of phase with strong ENSO events and, for potential temperature at both M2 and M3, $|r_{\text{NINO3.4}}| \geq |r_{\text{SAM}}|$. Instead, the primary role of the SAM on this time scale might be in modulating the high-latitude response to ENSO.

[51] *Fogt et al.* [2011] provide a reasonable mechanism for the modulation of ENSO by SAM, the crux being that during favorable phase relationships (Figure 1), the ADP teleconnection mechanism is strengthened. Once established, the ADP is maintained in part by cyclone activity associated with the polar front jet [*Yuan*, 2004]. We find that the first EOF of zonal wind anomalies at 300 mb between 70°S and 25°S during our period of study reveals an enhanced polar front jet with a reduced subtropical jet (not shown) and its principal component correlates significantly with the SAM (r = 0.79). Then, the SAM is capable of modulating the mechanisms both enacting and maintaining the ADP. While the first mode of our MEOF analysis (Figure 5) clearly represents the SAM and its principal component correlates very well with the SAM index (r = 0.81), the ENSO-driven PSA imprint is overwhelming with a spatial pattern more like a La Niña/+SAM composite

Figure 10. (a) Six month running mean of meridional wind anomalies (dashed line) at 52.5°W, 75°S and sea ice concentration anomalies averaged over the shelf in the western Weddell Sea (solid line). Blue shading marks calendar years when more shelf water is formed while red shading years when less is formed, both based on the principles of mechanism I. (b) Temperature anomalies at M2 and M3, where blue indicates calendar years of anomalously cold pulses and red indicates calendar years of anomalously warm pulses (mean temperature anomaly for that year, negative or positive, respectively). (c) Schematic of the relationship between winds, summer sea ice, and dense shelf water formation in winter.

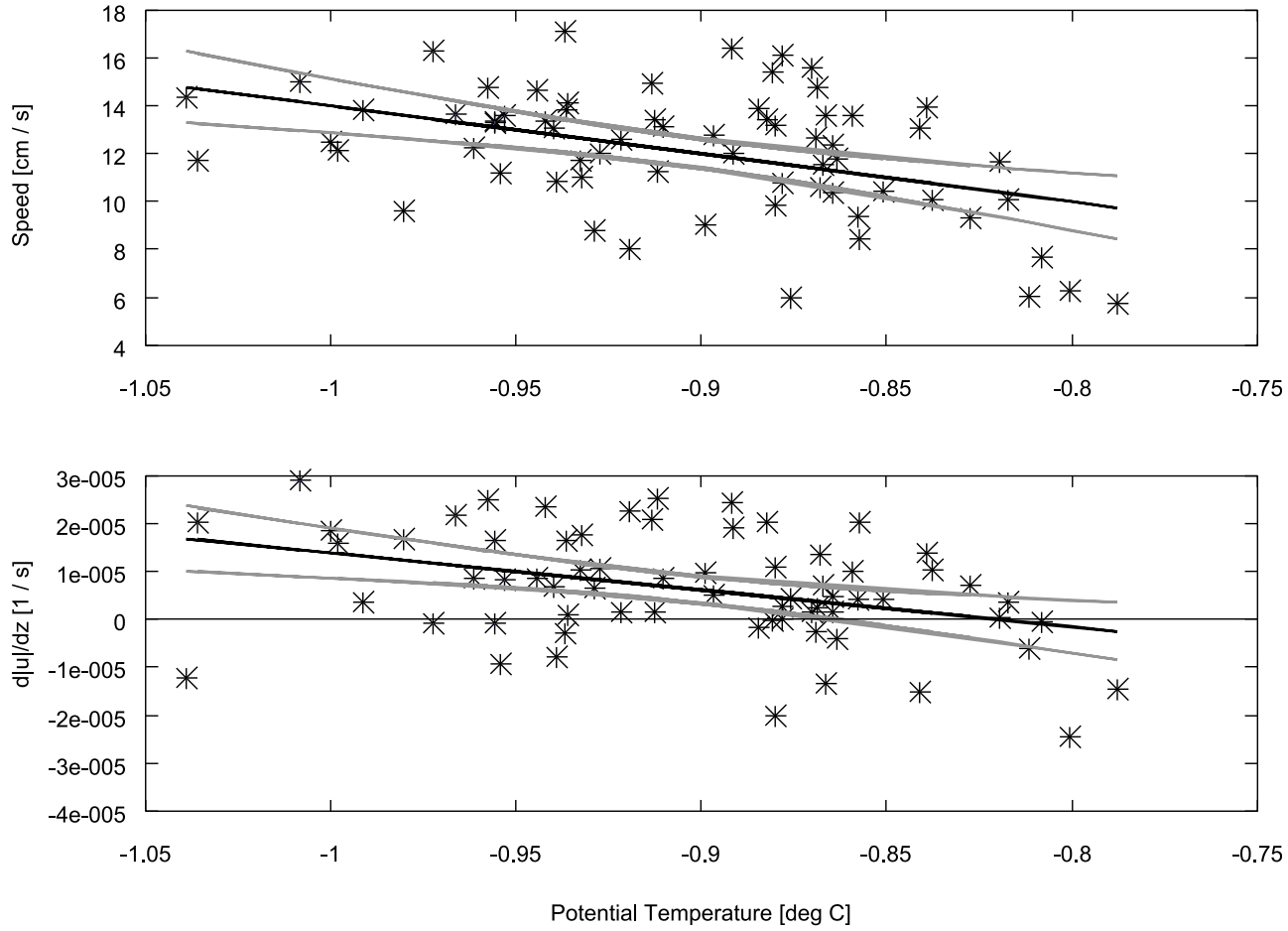

Figure 12. (top) Bottom speed at M3 and (bottom) estimated shear at M3 as functions of bottom potential temperature. Black lines indicate trend lines while gray curves indicate a 95% confidence interval. R values are −0.44 and −0.38 for speed and shear, respectively, and both are significant at a 99% level.

[*Fogt et al.*, 2011]. This confirms that our period of study is dominated by favorable phase occurrences of ENSO and SAM. The hierarchies of correlation values may suggest that such occurrences are necessary to sustain the anomalies required for anomalous dense water production.

[52] As for Mechanism II, our results suggest that a positive (negative) phase SAM corresponds to a colder (warmer) temperature anomaly 1–6 months later. The enhanced westerlies and the prevailing low pressure over the Weddell Gyre under a positive SAM act to promote a stronger mean wind stress curl. The correlations (for both the SAM at this time scale and the mean wind stress curl with potential temperature) might be low because the period of strongest anomalies observed at the moorings is one where the phases of ENSO and SAM are opposite as illustrated in Figure 1. While such a coincidence of the modes tends to reinforce the meridional wind and sea ice anomalies, the variability of gyre vigor is obfuscated by decreased (increased) cyclonic forcing from

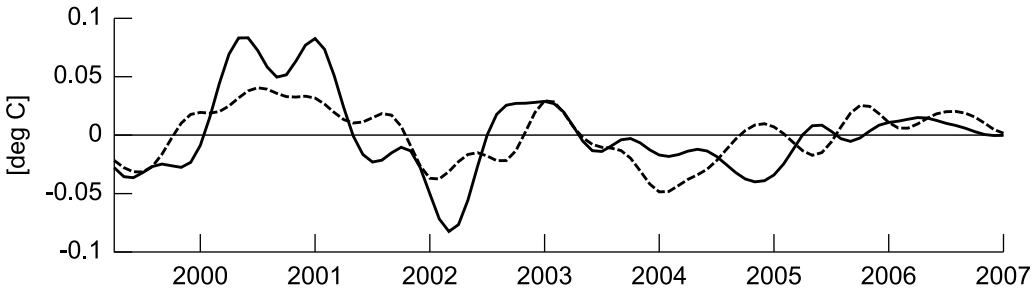

Figure 13. Actual bottom temperature anomalies at M3 (solid) and predicted temperature anomalies at M3 (dashed) from linear model described in section 4.3. The r value is 0.66, while the adjusted r value is 0.65.

cold (warm) ENSO anomalies with increased (decreased) cyclonic forcing from positive (negative) phase SAM anomalies competing for influence. As a result, the signal is much less distinct. There is no correlation with ENSO at this time scale so Mechanism II is probably primarily induced by the SAM.

[53] We conclude this discussion with a timeline of events to summarize the forcing process. In the austral summer (~18–21 months before pulse) a warm ENSO event may develop. A teleconnection to high latitudes develops ADP anomalies in sea ice and winds that may be enhanced by a negative phase SAM. Associated cold winds through the summer and fall increase offshore advection of sea ice to provide a greater open area at the ice shelf edge (~14–18 months before pulse). By austral winter these ADP anomalies may persist, allowing the greater area of open water to freeze, increasing brine rejection and increasing the shelf's supply of dense water (~12 months before pulse). Major export of dense water is constrained to occur in austral spring/summer [*Gordon et al.*, 2010] (~4–8 months before pulse), during which a positive phase SAM may enhance the cyclonic circulation, dome the pycnocline and upper isopycnals toward the shelf edge, and facilitate this export. Finally, the cold anomaly is advected to the moorings. The opposite holds for a warm anomaly.

5. Conclusions

[54] In an 8-year time series of potential temperature documenting the outflow of the Weddell Gyre south of the South Orkney Islands, we found substantial interannual variability with anomalously cold pulses in austral winters of 1999 and 2002 with a bypassed cold pulse in austral winter 2000. The temperature anomalies suggest an influence from ENSO at 14–20 months lead time and influences from the SAM at 14–20 months lead time as well as 1–6 months lead time. A MEOF analysis of surface forcings again suggests that these are the dominant modes of climate variability in the spatial and temporal scales of interest and that these are appropriate time scales for forcing.

[55] The enhanced northward meridional wind associated with warm ENSO events and the nonannular component of the negative phase SAM is associated with increased advection of sea ice for more (and/or broader) coastal polynyas and increased open sea area over the continental shelf for more freezing and brine rejection, all leading to a greater volume of dense shelf water available. The weakened (or reversed) meridional wind associated with cold ENSO events and the nonannular component of positive phase SAM is associated with the opposite conditions. Such forcings have impact on WSBW properties 14–20 months later. The enhanced cyclonic forcing associated with the annular component of positive phase SAM yields domed isopycnals due to a more vigorous Weddell Gyre whose consequences permit increased outflow. Such a forcing has impact on WSBW properties 1–6 months later.

[56] While the physical mechanisms enacting the temperature anomalies are clear, the links between large-scale climate modes and these anomalies are less so. Nevertheless, a linear model suggests that at least the sign of WSBW temperature anomalies can be predicted from values of the climate indices. An assessment of surface anomalies, correlation values, and their lag times suggests that the ENSO more likely directly drives the ADP related anomalies while the SAM modulates this impact. The SAM may additionally impact the mean wind stress curl over the gyre. It is very likely that the observed anomalies in WSBW temperature are responses to different contributions from each of the above forcings, as well as to internal climate variability, intermittent activities of local icebergs and spatially varying sources, and the interaction of all of the above with a residence time of several years. It also appears that the regional response to extrapolar forcing is strong only when the forcing signal is large. Without large ENSO and SAM events after 2004, the WSBW signal is reduced to its seasonal variability (Figures 1 and 3). This suggests that for the forcing mechanisms proposed to be fully realized, the climate anomalies need to be large in magnitude and possibly also in favorable phases.

Appendix A

A1. Lagged Correlations

[57] Given the short nature of the temperature time series involved, maximizing the number of points used in computing the cross-correlation function (CCF) is important to enhance both significance and physical interpretation. The cross-correlation function for two time series of equal length n involves summing over n-|k| pairs of data at each lag k, where k is an integer between [1-n, n-1]. Necessarily, this precludes the possibility of capturing the influence of the sustained large-amplitude climate variability (Figure 1) occurring prior to our earliest temperature observations. This variability is central to our hypothesis.

[58] Because we are correlating our temperature time series with forcing time series that are subsets of longer series, it is possible to compute the CCF using two time series of unequal length. The net effect of this procedure is to create a "sliding window" in which every lagged correlation involves n_T points (the number of points in the temperature time series). In computing the CCF in this case, we cannot recalculate the mean and standard deviation of the forcing time series in each window because this violates the assumption of stationarity. On the other hand, if the forcing time series is much longer than the temperature time series, the mean and standard deviation of the longer forcing time series may not be representative of the surface and large-scale climate forcing over the period of temperature observation and may lead to artificially high or low r values. Therefore we do not use such a method.

[59] As a compromise, for all lagged correlations in this study we use the standard lagged correlation of two-time series of equal length while extending both temperature time series back 24 months to April 1997 by substituting the respective climatology over this period. We stress that the same method without "padding" and the methods using time series of unequal length are able to reproduce the features of this method's CCF that serve as the basis for our physical interpretations. All correlations are biased, or divided by (n-1), so that the CCF decays toward zero at large lags.

A2. Bootstrap Method for Correlation and Lag Significance

[60] For all correlations, we generate 1000 random temperature time series to evaluate a random response to the

surface and large-scale climate forcing. The random time series are produced so as to maintain the spectral color of the original temperature time series. First, the discrete Fourier transform of the temperature time series T is computed and the amplitude of this complex series A_{orig} is kept. Then, the phase of this complex series for the positive frequencies is generated from a pseudorandom number generator scaled to the range $[-\pi, +\pi]$ while the phase for the negative frequencies is derived from this distribution. Calling the random phases θ_{rand}, we create a new complex series A_{orig}*exp ($i\theta_{rand}$). Because of our definition of θ_{rand}, this complex series preserves the Hermitian symmetry demanded of real-valued time series. We take the inverse Fourier transform of this complex series to get T_{rand}. The process is repeated 1000 times for the time series at M2 and M3.

[61] These random temperature time series are correlated with the surface or climate time series of interest at the full range of lags. For each lag, the sorted distribution of 1000 r values is used to create significance levels via a percentile approach. For example, the 25th and 975th r values determine the bounds for the 95% level.

[62] To evaluate the significance of the lag time, we evaluate these random lagged correlations in tandem with the equivalent lagged correlations of the real temperature time series. We first note at what relevant lag time the real CCF provides max(|r|). Then, among the 1000 random correlations, we note how many times each lag time provides max(|r|) of the corresponding CCF. This frequency divided by 1000 and subtracted from 1 provides the "significance of the lag time" or literally how confident we are that our observed lag time did not provide max(|r|) by chance. The usefulness of this statistic is that for high significance values, we are confident that the observed lag time is not due to some intrinsic quality of the temperature time series.

[63] **Acknowledgments.** We would like to thank the two anonymous reviewers whose insightful comments greatly improved this manuscript. We would also like to thank Doug Martinson for his help in developing the bootstrapping methods used. This research was funded in full or in part under the Cooperative Institute for Climate Applications Research (CICAR) award number NA08OAR4320754 from the National Oceanic and Atmospheric Administration, U.S. Department of Commerce. The statements, findings, conclusions, and recommendations are those of the author(s) and do not necessarily reflect the views of the National Oceanic and Atmospheric Administration or the Department of Commerce. Additionally, McKee was supported in part by the LDEO Climate Center, Yuan was supported by NSF grants ANT 07–39509 and OPP 02–30284, and Dong was supported by the Program on Sustaining Science and Technology (grant 2006BAB18B02) from the Ministry of Science and Technology, China. Lamont-Doherty Earth Observatory contribution 7455.

References

Ackley, S. F., C. A. Geiger, J. C. King, E. C. Hunke, and J. Comiso (2001), The Ronne polynya of 1997/98: Observations of air-ice-ocean interaction, *Ann. Glaciol.*, *33*, 425–429, doi:10.3189/172756401781818725.

Bailey, R., A. Gronell, H. Phillips, G. Meyers, and E. Tanner (1993), *CSIRO Cookbook for Quality Control of Expendable Bathythermograph (XBT) Data*, *Rep. 220*, CSIRO Mar. Lab., Hobart, Tas., Australia.

Barber, M., and D. Crane (1995), Current flow in the north-west Weddell Sea, *Antarct. Sci.*, *7*, 39–50, doi:10.1017/S0954102095000083.

Beckmann, A., H. H. Hellmer, and R. Timmermann (1999), A numerical model of the Weddell Sea: Large-scale circulation and water mass distribution, *J. Geophys. Res.*, *104*(C10), 23,375–23,391, doi:10.1029/1999JC900194.

Carmack, E. C., and T. D. Foster (1975), On the flow of water out of the Weddell Sea, *Deep Sea Res. Oceanogr. Abstr.*, *22*, 711–724, doi:10.1016/0011-7471(75)90077-7.

Comiso, J. C., D. J. Cavalieri, C. L. Parkinson, and P. Gloersen (1997), Passive microwave algorithms for sea ice concentration: A comparison of two techniques, *Remote Sens. Environ.*, *60*(3), 357–384, doi:10.1016/S0034-4257(96)00220-9.

Drinkwater, M. R., D. Long, and D. Early (1995), Comparison of variations in sea-ice formation in the Weddell Sea with seasonal bottom-water outflow data, in *1995 International Geoscience and Remote Sensing Symposium, IGARSS '95: Quantitative Remote Sensing for Science and Applications*, vol. 1, edited by T. I. Stein, pp. 402–404, IEEE Comput. Soc. Press, Silver Spring, Md.

Fahrbach, E., G. Rohardt, N. Scheele, M. Schroeder, V. Strass, and A. Wisotzki (1995), Formation and discharge of deep and bottom water in the northwestern Weddell Sea, *J. Mar. Res.*, *53*(4), 515–538, doi:10.1357/0022240953213089.

Fahrbach, E., M. Hoppema, G. Rohardt, M. Schröder, and A. Wisotzki (2004), Decadal-scale variations of water mass properties in the deep Weddell Sea, *Ocean Dyn.*, *54*, 77–91, doi:10.1007/s10236-003-0082-3.

Fogt, R. L., D. H. Bromwich, and K. M. Hines (2011), Understanding the SAM influence on the South Pacific ENSO teleconnection, *Clim. Dyn.*, *36*, 1555–1576, doi:10.1007/s00382-010-0905-0.

Foldvik, A., T. Gammelsrød, and T. Tørresen (1985), Circulation and water masses on the southern Weddell Sea shelf, in *Oceanology of the Antarctic Continental Shelf*, *Antarct. Res. Ser.*, vol. 43, edited by S. S. Jacobs, pp. 5–20, AGU, Washington, D. C.

Foster, T. D., and E. C. Carmack (1976), Frontal zone mixing and Antarctic Bottom Water formation in the southern Weddell Sea, *Deep Sea Res. Oceanogr. Abstr.*, *23*, 301–317, doi:10.1016/0011-7471(76)90872-X.

Foster, T. D., and J. H. Middleton (1980), Bottom water formation in the western Weddell Sea, *Deep Sea Res., Part A*, *27*, 367–381, doi:10.1016/0198-0149(80)90032-1.

Gill, A. E. (1973), Circulation and bottom water production in the Weddell Sea, *Deep Sea Res. Oceanogr. Abstr.*, *20*, 111–140, doi:10.1016/0011-7471(73)90048-X.

Gong, D., and S. Wang (1999), Definition of Antarctic Oscillation Index, *Geophys. Res. Lett.*, *26*(4), 459–462, doi:10.1029/1999GL900003.

Gordon, A. L. (1998), Western Weddell Sea thermohaline stratification, in *Ocean, Ice and Atmosphere: Interactions at the Antarctic Continental Margin*, *Antarct. Res. Ser.*, vol. 75, edited by S. S. Jacobs and R. Weiss, pp. 215–240, AGU, Washington, D. C.

Gordon, A. L., B. A. Huber, H. H. Hellmer, and A. Ffield (1993), Deep and bottom water of the Weddell Sea's western rim, *Science*, *262*, 95–97, doi:10.1126/science.262.5130.95.

Gordon, A. L., M. Visbeck, and B. Huber (2001), Export of Weddell Sea Deep and Bottom Water, *J. Geophys. Res.*, *106*(C5), 9005–9017, doi:10.1029/2000JC000281.

Gordon, A. L., B. Huber, D. McKee, and M. Visbeck (2010), A seasonal cycle in the export of bottom water from the Weddell Sea, *Nat. Geosci.*, *3*(8), 551–556, doi:10.1038/ngeo916.

Grumbine, R. W. (1991), A model of the formation of high-salinity shelf water on polar continental shelves, *J. Geophys. Res.*, *96*(C12), 22,049–22,062, doi:10.1029/91JC00531.

Heywood, K. J., A. C. Naveira Garabato, and D. P. Stevens (2002), High mixing rates in the abyssal Southern Ocean, *Nature*, *415*, 1011–1014, doi:10.1038/4151011a.

Holland, M. M., C. M. Bitz, and E. C. Hunke (2005), Mechanisms forcing an Antarctic dipole in simulated sea ice and surface ocean conditions, *J. Clim.*, *18*, 2052–2066, doi:10.1175/JCLI3396.1.

Huhn, O., H. H. Hellmer, M. Rhein, C. B. Rodehacke, W. Roether, M. P. Schodlok, and M. Schröder (2008), Evidence of deep- and bottom-water formation in the western Weddell Sea, *Deep Sea Res., Part II*, *55*, 1098–1116, doi:10.1016/j.dsr2.2007.12.015.

Jullion, L., S. C. Jones, A. C. Naveira Garabato, and M. P. Meredith (2010), Wind-controlled export of Antarctic Bottom Water from the Weddell Sea, *Geophys. Res. Lett.*, *37*, L09609, doi:10.1029/2010GL042822.

Kerr, R., M. M. Mata, and C. A. E. Garcia (2009), On the temporal variability of the Weddell Sea Deep Water masses, *Antarct. Sci.*, *21*, 383–400, doi:10.1017/S0954102009001990.

Klatt, O., E. Fahrbach, M. Hoppema, and G. Rohardt (2005), The transport of the Weddell Gyre across the Prime Meridian, *Deep Sea Res., Part II*, *52*, 513–528, doi:10.1016/j.dsr2.2004.12.015.

Lefebvre, W., and H. Goosse (2005), Influence of the Southern Annular Mode on the sea ice-ocean system: The role of the thermal and mechanical forcing, *Ocean Sci.*, *1*, 145–157, doi:10.5194/os-1-145-2005.

Lefebvre, W., H. Goosse, R. Timmermann, and T. Fichefet (2004), Influence of the Southern Annular Mode on the sea-ice-ocean system, *J. Geophys. Res.*, *109*, C09005, doi:10.1029/2004JC002403.

Liu, J., X. Yuan, D. Rind, and D. G. Martinson (2002), Mechanism study of the ENSO and southern high latitude climate teleconections, *Geophys. Res. Lett.*, *29*(14), 1679, doi:10.1029/2002GL015143.

Marshall, G. J. (2003), Trends in the Southern Annular Mode from observations and reanalyses, *J. Clim.*, *16*, 4134–4143, doi:10.1175/1520-0442(2003)016<4134:TITSAM>2.0.CO;2.

Marshall, G. J., and S. A. Harangozo (2000), An appraisal of NCEP/NCAR reanalysis MSLP data viability for climate studies in the South Pacific, *Geophys. Res. Lett.*, *27*(19), 3057–3060, doi:10.1029/2000GL011363.

Martinson, D. G. (1990), Evolution of the Southern Ocean winter mixed layer and sea ice: Open ocean deepwater formation and ventilation, *J. Geophys. Res.*, *95*(C7), 11,641–11,654, doi:10.1029/JC095iC07p11641.

Martinson, D. G., and R. A. Iannuzzi (1998), Antarctic Ocean-ice interaction: Implications from ocean bulk property distributions in the Weddell Gyre, in *Antarctic Sea Ice: Physical Processes, Interactions and Variability*, *Antarct. Res. Ser.*, vol. 74, edited by M. Jeffries, pp. 243–271, AGU, Washington, D. C.

Martinson, D. G., and R. A. Iannuzzi (2003), Spatial/temporal patterns in Weddell gyre characteristics and their relationship to global climate, *J. Geophys. Res.*, *108*(C4), 8083, doi:10.1029/2000JC000538.

Mensch, M., R. Bayer, J. L. Bullister, P. Schlosser, and R. Weiss (1996), The distribution of tritium and CFCs in the Weddell Sea during the mid 1980s, *Prog. Oceanogr.*, *38*, 377–388, doi:10.1016/S0079-6611(97)00007-4.

Meredith, M. P., A. C. Naveira Garabato, A. L. Gordon, and G. C. Johnson (2008), Evolution of the deep and bottom waters of the Scotia Sea, Southern Ocean, 1995–2005, *J. Clim.*, *21*(13), 3327–3343, doi:10.1175/2007JCLI2238.1.

Muench, R. D., L. Padman, S. L. Howard, and E. Fahrbach (2002), Upper ocean diapycnal mixing in the northwestern Weddell Sea, *Deep Sea Res., Part II*, *49*, 4843–4861, doi:10.1016/S0967-0645(02)00162-5.

Nicholls, K. W., and S. Østerhus (2004), Interannual variability and ventilation timescales in the ocean cavity beneath Filchner-Ronne Ice Shelf, Antarctica, *J. Geophys. Res.*, *109*, C04014, doi:10.1029/2003JC002149.

Nuñez-Riboni, I., and E. Fahrbach (2009), Seasonal variability of the Antarctic Coastal Current and its driving mechanisms in the Weddell Sea, *Deep Sea Res., Part I*, *56*, 1927–1941, doi:10.1016/j.dsr.2009.06.005.

Orsi, A. H., W. D. Nowlin Jr., and T. Whitworth III (1993), On the circulation and stratification of the Weddell Gyre, *Deep Sea Res., Part I*, *40*, 169–203, doi:10.1016/0967-0637(93)90060-G.

Padman, L., S. Howard, and R. Muench (2006), Internal tide generation along the South Scotia Ridge, *Deep Sea Res., Part II*, *53*, 157–171, doi:10.1016/j.dsr2.2005.07.011.

Raphael, M. N. (2004), A zonal wave 3 index for the Southern Hemisphere, *Geophys. Res. Lett.*, *31*, L23212, doi:10.1029/2004GL020365.

Raphael, M. N. (2007), The influence of atmospheric zonal wave three on Antarctic sea ice variability, *J. Geophys. Res.*, *112*, D12112, doi:10.1029/2006JD007852.

Rind, D., M. Chandler, J. Lerner, D. G. Martinson, and X. Yuan (2001), Climate response to basin-specific changes in latitudinal temperature gradients and implications for sea ice variability, *J. Geophys. Res.*, *106*(D17), 20,161–20,173, doi:10.1029/2000JD900643.

Schroder, M., and E. Fahrbach (1999), On the structure and the transport of the eastern Weddell Gyre, *Deep Sea Res., Part II*, *46*, 501–527, doi:10.1016/S0967-0645(98)00112-X.

Simmonds, I., and J. C. King (2004), Global and hemispheric climate variations affecting the Southern Ocean, *Antarct. Sci.*, *16*, 401–413, doi:10.1017/S0954102004002226.

Smith, S. D. (1988), Coefficients for sea surface wind stress, heat flux, and wind profiles as a function of wind speed and temperature, *J. Geophys. Res.*, *93*(C12), 15,467–15,472, doi:10.1029/JC093iC12p15467.

Stammerjohn, S. E., D. G. Martinson, R. C. Smith, X. Yuan, and D. Rind (2008), Trends in Antarctic annual sea ice retreat and advance and their relation to El Niño-Southern Oscillation and Southern Annular Mode variability, *J. Geophys. Res.*, *113*, C03S90, doi:10.1029/2007JC004269.

Thompson, D. W. J., and S. Solomon (2002), Interpretation of recent Southern Hemisphere climate change, *Science*, *296*, 895–899, doi:10.1126/science.1069270.

Thompson, D. W. J., and J. M. Wallace (2000), Annular modes in the extratropical circulation, part I, Month-to-month variability, *J. Clim.*, *13*, 1000–1016, doi:10.1175/1520-0442(2000)013<1000:AMITEC>2.0.CO;2.

Timmermann, R., H. H. Hellmer, and A. Beckmann (2002), Simulations of ice-ocean dynamics in the Weddell Sea: 2. Interannual variability 1985–1993, *J. Geophys. Res.*, *107*(C3), 3025, doi:10.1029/2000JC000742.

Toggweiler, J. R., and B. Samuels (1995), Effect of sea ice on the salinity of Antarctic Bottom Waters, *J. Phys. Oceanogr.*, *25*, 1980–1997, doi:10.1175/1520-0485(1995)025<1980:EOSIOT>2.0.CO;2.

von Gyldenfeldt, A.-B., E. Fahrbach, M. A. Garcia, and M. Schroder (2002), Flow variability at the tip of the Antarctic Peninsula, *Deep Sea Res., Part II*, *49*, 4743–4766, doi:10.1016/S0967-0645(02)00157-1.

Weppernig, R., P. Schlosser, S. Khatiwala, and R. G. Fairbanks (1996), Isotope data from Ice Station Weddell: Implications for deep water formation in the Weddell Sea, *J. Geophys. Res.*, *101*(C11), 25,723–25,739, doi:10.1029/96JC01895.

Yuan, X. (2004), ENSO-related impacts on Antarctic sea ice: A synthesis of phenomenon and mechanisms, *Antarct. Sci.*, *16*(4), 415–425, doi:10.1017/S0954102004002238.

Yuan, X., and C. Li (2008), Climate modes in southern high latitudes and their impacts on Antarctic sea ice, *J. Geophys. Res.*, *113*, C06S91, doi:10.1029/2006JC004067.

Yuan, X., and D. G. Martinson (2000), Antarctic sea-ice extent variability and its global connectivity, *J. Clim.*, *13*, 1697–1717, doi:10.1175/1520-0442(2000)013<1697:ASIEVA>2.0.CO;2.

Yuan, X., and D. G. Martinson (2001), The Antarctic dipole and its predictability, *Geophys. Res. Lett.*, *28*(18), 3609–3612, doi:10.1029/2001GL012969.

Yuan, X., D. G. Martinson, and W. T. Liu (1999), Effect of air-sea-ice interaction on Southern Ocean subpolar storm distribution, *J. Geophys. Res.*, *104*(D2), 1991–2007, doi:10.1029/98JD02719.

Yuan, X., D. G. Martinson, and Z. Dong (2004), Upper ocean thermohaline structure and its temporal variability in the southeast Indian Ocean, *Deep Sea Res., Part I*, *51*, 333–347, doi:10.1016/j.dsr.2003.10.005.

Z. Dong, Polar Research Institute of China, 451 Jinqiao Rd., Shanghai, 200129, China.

A. L. Gordon, B. A. Huber, D. C. McKee, and X. Yuan, Lamont-Doherty Earth Observatory, Columbia University, 61 Rte. 9W, Palisades, NY 10964, USA. (dcm2117@columbia.edu)